Numerical Investigation on the Progressive Collapse Behavior of Precast Reinforced Concrete Frame Sub-assemblages

Citation for published version:
Feng, D-C, Wu, G & Lu, Y 2018, 'Numerical Investigation on the Progressive Collapse Behavior of Precast Reinforced Concrete Frame Sub-assemblages', *Journal of Performance of Constructed Facilities*, vol. 32, no. 3, 04018027, pp. 1-14.

Published In:
Journal of Performance of Constructed Facilities

Numerical Investigation on the Progressive Collapse Behavior of Precast Reinforced Concrete Frame Sub-assemblages

De-Cheng Feng[1], Gang Wu[2], and Yong Lu[3]

[1]Key Laboratory of Concrete and Prestressed Concrete Structures of the Ministry of Education, Southeast University, 2 Sipailou, Nanjing 210096, China

[2]Key Laboratory of Concrete and Prestressed Concrete Structures of the Ministry of Education, Southeast University, 2 Sipailou, Nanjing 210096, China, with corresponding author. Email: g.wu@seu.edu.cn

[3]Institute for Infrastructure and Environment, School of Engineering, The University of Edinburgh, Edinburgh EH9 3JL, UK

ABSTRACT

This paper presents a numerical investigation of the progressive collapse behavior of the precast reinforced concrete (RC) frame sub-assemblages. An efficient numerical model for the precast RC frame sub-assemblages under progressive collapse is developed based on OpenSEES software, where the fiber beam element is used for the beams and columns and the Joint2D element is used for the beam-to-column connections. To consider the significant bond-slip effect inside the joint core of the precast RC frame sub-assemblages, the stress-slip relationship for reinforcement bars with different embedded lengths is derived and used to generate the force-deformation relation for the springs incorporated in the Joint2D element. The numerical model is validated through comparisons with the experimental results of RC sub-assemblages subjected to column removal scenarios in terms of load-displacement curve, compressive arch action, catenary action capacity, etc. Finally systematic parametric studies are conducted based on the validated numerical model to investigate the influences of some typical parameters that involved in precast RC structures on the progressive collapse capacity of the sub-assemblages.

Keywords: progressive collapse, precast, RC frame sub-assemblages, numerical simulation, OpenSEES

INTRODUCTION

Progressive collapse of reinforced concrete (RC) structures has caught widespread attentions around the world in recent years, since great loss of public properties and human lives has been caused by progressive collapse of structures, and there has been an increasing trend of extreme events due to malicious attacks, accidental gas explosion and vehicle impact, etc.(Ellingwood 2006). To mitigate the progressive collapse risk of RC structures, some specific methods have been developed in various design codes and guidelines, e.g., General Service Administration (GSA) 2013 (GSA 2013) and Department of Defense (DoD) 2013 (DoD 2013). Among the proposed design methods, the alternate load path (ALP) method is the most commonly used one due to its efficiency and ease of operation (Pham et al. 2016). With this method, one middle column will be removed to check whether the remaining structure can bridge over the missing column. Although simply removing one column in the ALP method does not simulate the real initial damage scenario (a complete removal of a column is rarely seen in real incidents), it is considered as an effective way to assess the progressive collapse potential.

In light of the fundamental concepts of ALP approach, several experimental tests of RC beam-column sub-assemblages subjected to column removal scenarios have been conducted in the literature to investigate their progressive collapse resistance, i.e., the work done by Sasani and Kropelnicki (Sasani and Kropelnicki 2008), Yi et al. (Yi et al. 2008), Su et al. (Su et al. 2009), Yap and Li (Yap and Li 2011), Qian and Li (Qian and Li 2012), Yu and Tan (Yu and Tan 2013), Ren et al. (Ren et al. 2016), Lu et al. (Lu et al. 2016) and Qian et al. (Qian et al. 2016), etc. However, although experimental studies can provide first-hand results of RC frame sub-assemblages against progressive collapse, conducting such experiments are generally very costly and time consuming. Furthermore, due to the constraints of the experimental facilities and space, among other factors, it is impractical to investigate the influence of a variety of parameters on the progressive collapse behavior using physical experiments.

On the other hand, many numerical models have also been developed to study the progressive collapse behavior of RC frame sub-assemblages. Generally, the models may be grouped into three categories: the detailed finite element models, the fiber element-based models and the macro component-based models. Detailed finite element models (Sasani et al. 2011; Qian and Li 2011; Bao et al. 2012; Pham et al. 2016) usually adopt three-dimensional (3D) solid elements to simulate the behavior of an RC sub-assemblage, and the detailed local responses including concrete cracking and crushing, steel yielding and fracture, can be obtained. However, the computational effort of this approach is extremely demanding and oftentimes some convergence issues may also arise. Fiber element-based models (Valipour and Foster 2010; Li et al. 2011; Brunesi and Nascimbene 2014; Brunesi et al. 2015; Feng et al. 2016a; Yu et al. 2016; Brunesi and Parisi 2017) use fiber beam-column elements with co-rotational formulation to model the structure, in which the large deformation effect is well considered. This approach is much faster than using detailed finite element models, and the numerical accuracy in terms of the global response can also be guaranteed (Li et al. 2016a; Li et al. 2016b). However, some specific failure modes, e.g, bong-slip and bar fracture, cannot be reflected. The macro component-based models (Bao et al. 2008; Yu and Tan 2014) strive to achieve an adequate balance between the analysis accuracy and computational efficiency. In this type of models, fiber elements are still used to model beams and columns, but additional component-based joint model consisting of series of springs is introduced to represent the essential mechanisms of a beam-to-column connection; thus local failure in the joint region such as the bar slip and fracture can be incorporated. For these reasons, the macro component-based models are deemed more suitable for the progressive collapse analysis of RC frame assemblages.

So far the existing studies, either experimental or numerical, have mainly focused on the monolithic RC structures, while little attention has been paid on the progressive collapse capacity of precast RC structures. Actually, the precast structures are now widely used around the world due to various advantages such as the product quality, construction speed, and so on. Especially in rapidly developing countries like China, there is a great demand for precast structures due to the rapid process of urbanization. Therefore, there is an urgent need to study the progressive collapse behavior of precast structures. Kang and Tan (Kang and Tan 2015a; Kang and Tan 2017) conducted a set of experiments to investigate the progressive collapse capacity of precast sub-assemblages, and some special features that are unique in precast structures, e.g., discontinuous reinforcement, were also analyzed. However, no numerical model has been developed for precast RC sub-assemblages under a progressive collapse scenario up till now. Compared with the monolithic RC structures, the bond-slip effect is particularly significant in precast structures since the post-cast concrete quality can hardly be guaranteed (Kang and Tan 2015b), and therefore careful handling of this important feature is required in a numerical model.

Based on the above-mentioned aspects, this paper aims at developing an efficient numerical model for precast RC frame sub-assemblages against progressive collapse based on the software OpenSEES, and subsequently performing systemic parametric studies to investigate the progressive collapse behavior of precast sub-assemblages. First the numerical model is introduced in detail, where the fiber beam element is used for the beams and columns and the Joint2D element is used for the beam-to-column connections. In particular, an analytical stress-slip model is derived for the beam reinforcement in the middle joint of a precast sub-assemblage. The developed numerical model is then validated through comparison with the experimental results of the precast sub-assemblages under a column removal scenario. With the validated numerical model, systematic parametric studies are conducted to study the influences of some unique parameters in precast RC structures on its progressive collapse performance.

PROGRESSIVE COLLAPSE MODELING APPROACH BASED ON OPENSEES

As mentioned before, the progressive collapse process of precast frame sub-assemblages involves several complex behavioral developments of the structure, including material nonlinearity, geometrical nonlinearity, bond-slip effect, and bar fracture. Furthermore, the force transfer mechanism from beams to columns through the connection part should also be clearly represented in the numerical model. Although a detailed model involving continuum solid elements can capture these local responses, the numerical efficiency and convergence issue remain a problem. Therefore, an alternative marco-level element approach based on fiber element and Joint2D element (Altoontash

2004), which are available in OpenSEES, is adopted in this paper to simulate the progressive collapse behavior of precast sub-assemblages.

Proposed modeling approach for precast sub-assemblage

In the proposed numerical modeling of the precast sub-assemblages, conventional displacement-based (DB) fiber beam-column elements are used to simulate the beams and columns, while Joint2D element is used to model the beam-to-column connection, as indicated in Fig. 1. The fiber element is based on co-rotational formulation to include large deformation effect, and Gauss-Legendre quadrature is used in the element. The cross-section of the element is divided into concrete and reinforcement fibers, and each fiber has its own uniaxial constitutive law. Different fibers can have different constitutive laws, and thus the properties of precast and post-cast concrete can be assigned separately and the confinement effect provided by stirrups can also be considered. The concrete damage-plasticity model (ConcreteD), which is implemented in OpenSEES and recommended in a Chinese code for design of concrete structures (Ministry of Construction of the People's Republic of China 2010), and the bilinear steel model (Steel01) are adopted for concrete and reinforcement fibers, respectively. The details for the two material models are given in Appendix I and II.

The Joint2D element is developed by Altoontash (Altoontash 2004), which is actually a simplified version of the BeamColumnJoint element in OpenSEES (Lowes and Altoontash 2003), and large deformation effect can also be accounted for in the model. Although similar component-based joint models are also proposed in the literature (Bao et al. 2008; Yu and Tan 2013; Yu and Tan 2014) to model the progressive collapse behavior of RC sub-assemblages, they seem to be more complicated and need complex calibration of the component properties. The proposed element herein modifies the original Joint2D element to suit for a progressive collapse analysis, and consists of five spring components, representing the shear distortion of the joint panel and the moment-rotation behavior including the bar bond-slip effect of the section at the four ends of beams and columns, respectively. The five spring components are defined with uniaxial force-deformation relations (Altoontash 2004). For the central shear spring, usually the shear stress-strain relation $\tau - \gamma$ is determined based on the modified compression field theory (MCFT) (Vecchio and Collins 1986) or the softened truss model (STM) (Hsu 1988), and then it is converted to the equivalent moment-rotation relation $M - \theta$ of the joint panel with the following expressions: $M = \tau V_J$, $\theta = \arctan \gamma$, where V_J is the volume of the panel. However, several studies indicate that there is no significant shear deformation of the joint panel when the sub-assemblage is under progressive collapse, since the joint is subjected to vertical displacement and restrained by the surrounding beam and columns (Bao et al. 2008; Yu and Tan 2013; Yu and Tan 2014; Rashidian et al. 2016). Hence, the shear spring is assumed to be elastic in this paper, enabling a rigid shear panel behavior. For the interface springs at the beam and column ends, which actually represents the member-end rotation due to bond-slip effect, the corresponding force-deformation relation is calibrated based on a fiber section analysis (unit length) with the stress-strain relation for the steel fibers replaced by the stress-slip relation (Altoontash 2004), and the bar fracture is considered through a Min-Max criterion material in OpenSEES (Feng et al. 2016a). Moreover, the column end springs can be further simplified as rigid since no failure would occur at the column-joint interface when the sub-assemblage is under a column removal scenario. The stress-slip relation of the steel fibers can be obtained from either experimental results or theoretical derivation, and the generated section force-deformation relationship is then simplified into a tri-linear relationship by getting the critical points and assigned to the springs, which can be done by the Hysteretic material model in OpenSEES, as shown in Fig. 2. A summary of the proposed modeling approach is given in Table 1.

It should be noted that in modelling the joint it is usually assumed that the rebar development length is sufficient (Altoontash 2004); however, this may be not true for precast structure, especially for the bottom reinforcement of the beam under a column removal scenario. Therefore, a stress-slip model for the reinforcement bars of the beam with different embedded lengths is derived in the next section to address this situation.

Analytical derivation of the stress-slip behavior of reinforcement

The bond-slip effect is an important factor that influences the progressive collapse behavior of the precast sub-assemblage, since the reinforcement may develop large strain under a column removal scenario and thereby bond failure could occur. Especially, this effect is even more significant for precast structures since the quality of the post-cast concrete in the joint core region cannot be guaranteed as the monolithic structures. Moreover, although some of the existing macro-models can account for bond-slip effect, there is commonly an associated assumption that the embedded length for bars is sufficient; consequently the applicability is restricted, especially for precast concrete structures.

In the present modeling approach introduced in the previous subsection, the bond-slip effect is considered through the beam interface springs in the Joint2D element, and the spring properties are calibrated through a unit length fiber section analysis discussed before. Hence, a stress-slip model is needed herein.

The bond-slip behavior of the beam reinforcement when subjected to progressive collapse actually depends on the anchorage type. Generally, three kinds of anchorage are used in precast RC structures, namely, continuous, lap-spliced and hooked, as shown in Fig. 3. The total slip s of the reinforcement is actually given by the integral of the strain distribution $\epsilon(x)$ along the embedded length L_{embd}, i.e.,

$$s = \int_0^{L_{embd}} \epsilon(x)\, dx \tag{1}$$

Assuming that the bond stress is a stepped distribution (Sezen and Setzler 2008), as shown in Fig. 3, the total slip of the reinforcement can be analytically derived based on the static equilibrium condition and Eq. (1). Denoting the strain at the loaded end as ϵ_s and the yielding strain as ϵ_y, the bond stress for elastic part ($\epsilon_s \leq \epsilon_y$) and plastic part ($\epsilon_s > \epsilon_y$) are defined as $u_{be} = 1.8\sqrt{f_c'}$ and $u_{by} = 0.5\sqrt{f_c'}$, respectively, where f_c' is the cubic compressive strength of concrete (Yu and Tan 2014). The detailed slip derivation for different anchorage types are given as follows:

* *For continuous bar* (Fig. 3(a))

  When a precast sub-assemblage is subjected to progressive collapse in a typical middle column removal scenario, the continuous reinforcement inside the joint will finally stress up to the center of the joint under catenary action, and the embedded length of the reinforcement actually equals half of the column width h_c, i.e., $L_{embd} = 0.5h_c$. The development of the slip can be divided into three stages. At first the bar is elastic and the corresponding developed elastic bond length L_{ed} can be determined by the force equilibrium

$$L_{ed} = \frac{f_s d_b}{4u_{be}} \tag{2}$$

where d_b is the bar diameter; f_s is the reinforcement stress. Then the slip is obtained through Eq. (1)

$$s = \int_0^{L_{ed}} \epsilon\left(x\right) dx = \frac{\epsilon_s}{2} L_{ed} \tag{3}$$

After that the bar yields but is not stressed up to the center, the yielded length L_{yd} is given by

$$L_{yd} = \frac{\left(f_s - f_y\right) d_b}{4u_{by}} \tag{4}$$

and the slip is computed as

$$s = \int_0^{L_{ed}} \epsilon\left(x\right) dx + \int_{L_{ed}}^{L_{yd}} \epsilon\left(x\right) dx = \frac{\epsilon_y}{2} L_{ed} + \frac{\epsilon_y + \epsilon_s}{2} L_{yd} \tag{5}$$

Finally, the reinforcement is stressed up to the center of the joint under catenary action, but the slip at the center point is still zero due to symmetry. The corresponding elastic developed length and yielded developed length are

$$L_{yd} = \frac{\left(f_s - f_y\right) d_b}{4u_{by}}, \quad L_{ed} = L_{embd} - L_{yd} \tag{6}$$

and the slip is

$$s = \int_0^{L_{ed}} \epsilon\left(x\right) dx + \int_{L_{ed}}^{L_{yd}} \epsilon\left(x\right) dx = \frac{\epsilon_{end} + \epsilon_y}{2} L_{ed} + \frac{\epsilon_y + \epsilon_s}{2} L_{yd} \tag{7}$$

where ϵ_{end} can be determined through similar triangle method. Note that no pull-out failure will occur in this case.

* *For lap-spliced and hooked bar* (Fig. 3(b) and 3(c))

Unlike the case with continuous bar, the bond stress of lap-spliced and hooked bar may develop until to the free-end; the strain and stress at the free-end should be zero and the strain profile should be modified to the blue dashed line in Fig. 4. The free-end slip (if any) should be also included in the total slip. The embedded length for lap-spliced bar is the realistic one, while for hooked bar, it can be modelled as a straight bar with an equivalent length of (Yu and Tan 2014)

$$L_{embd} = L^s_{embd} + 5d_b \tag{8}$$

where L^s_{embd} is the straight embedment length of the hooked bar.

According to the relation between the embedded length and developed bond length and the assumption discussed above, as shown in Fig. 4, the slip is derived as follows:

• If the bar embedded length is sufficient to develop full bond length L_d (Fig. 4(a)), the failure mode is bar fracture, the developed process of the bond stress involves two stages. At first the bar is elastic, and developed elastic bond length L_{ed} and corresponding slip are given by

$$L_{ed} = \frac{f_s d_b}{4u_{be}}, \quad s = \int_0^{L_{ed}} \epsilon(x)\, dx = \frac{\epsilon_s}{2} L_{ed} \tag{9}$$

Then the bar yields, and the yield length and slip are

$$L_{yd} = \frac{\left(f_s - f_y\right) d_b}{4u_{by}}, \quad s = \int_0^{L_{ed}} \epsilon(x)\, dx + \int_{L_{ed}}^{L_{yd}} \epsilon(x)\, dx = \frac{\epsilon_y}{2} L_{ed} + \frac{\epsilon_y + \epsilon_s}{2} L_{yd} \tag{10}$$

• If the bar embedded length is sufficient to develop elastic bond length but not sufficient to develop full bond length (Fig. 4(b)), the first two stages of slip evolution are the same with Eqs. (9) and (10) in last case. However, the bar will be stressed up to the free-end, and free end slip may occur. So the developed length and slip in this situation are expressed as

$$L_{yd} = \frac{\left(f_s - f_y\right) d_b}{4u_{by}}, \quad L_{ed} = L_{embd} - L_{yd} \tag{11}$$

$$s = s_0 + \int_0^{L_{ed}} \epsilon(x)\, dx + \int_{L_{ed}}^{L_{yd}} \epsilon(x)\, dx = s_0 + \frac{\epsilon_y}{2} L_{ed} + \frac{\epsilon_y + \epsilon_s}{2} L_{yd} \tag{12}$$

where s_0 is the free-end slip and can be determined by

$$s_0 = s_1 \left(\frac{u_e}{u_u}\right)^{2.5} \tag{13}$$

with

$$s_1 = \left(\frac{30}{f_c'}\right)^{0.5}, \quad u_e = \frac{f_{se} d_b}{4L_{edb}}, \quad u_u = \left(20 - \frac{d_b}{4}\right)\left(\frac{f_c'}{30}\right)^{0.5} \tag{14}$$

where s_1 is the ultimate slip at the free-end; u_e is the elastic bond stress at the free-end; u_u is the ultimate bond stress; f_{se} is the maximum bar stress ($\leq f_y$) in the elastic developed bond length. Note that if u_e reaches u_u ($s_0 \geq s_1$), the bar will fail by a pull-out mode.

• If the bar embedded length is even not sufficient to develop elastic bond length (Fig. 4(c)), at first it is still the same as Eq. (9), then the bar will be stressed up when the applied strain is even in the elastic stage; the developed elastic bond length is actually the full embedded length, i.e., $L_{ed} = L_{embd}$, thus the slip is

$$s = s_0 + \int_0^{L_{ed}} \epsilon(x)\, dx = s_0 + \frac{\epsilon_s}{2} L_{embd} \tag{15}$$

If there is no pull-out failure ($s_0 \geq s_1$) even when the bar yields at the loaded end, then the slip is the same as Eq. (12).

With the above equations, the reinforcement stress-slip relation can be obtained. Note that two kinds of bar failure modes may happen, namely, fracture failure ($\epsilon_s \geq \epsilon_u$) and pull-out failure

($s_0 \geq s_1$); here whichever mode is first reached will be treated as the failure of the bar. Meanwhile, the bond-slip effect is neglected for reinforcement under compression in this paper. In fact, when subjected to progressive collapse, the reinforcement will eventually undergo tension to develop catenary action, thus the bond-slip behavior under compression will have little influence on its global performance.

Nonlinear solution strategy

The numerical simulation of progressive collapse of precast sub-assemblage includes several extreme behaviors, i.e., material and geometrical nonlinearity, bar fracture etc. Therefore, some convergence issue may arise in the simulation and the numerical solution algorithm is a challenge aspect. To improve the numerical performance, a varying solution strategy is employed in this paper. The analysis starts with the full Newton-Raphson algorithm, which has the fastest convergence rate, and the convergence tolerance is set as 10^{-6} on the norm of energy increment. The maximum number of iterations for each time step is defined as 200. If the solution cannot be obtained in a single step, the analysis switches the algorithm in turn to modified Newton-Raphson method, Krylov Newton acceleration method and Newton line search method until the convergence is attained. If it still fails to obtain a solution, the iteration number is increased (i.e., 1000). If a solution still cannot be obtained, a larger tolerance is then adopted (i.e., 10^{-4}). After the convergence is obtained, all these settings are returned back to the default ones for the next step.

VALIDATION OF THE PROPOSED MODELING APPROACH

Overview of progressive collapse test on precast RC sub-assemblages

To validate the proposed numerical modeling approach for precast RC sub-assemblages, the experiments conducted by Kang and Tan's group (Kang and Tan 2015a; Kang et al. 2015) are simulated. The experiments were performed to investigate whether the precast sub-assemblages could develop catenary action under column removal, even though they could exhibit similar seismic performance as the monolithic structures. Totally six specimens, designed in accordance with Eurocode 2, were tested. The geometrical dimensions were kept the same, and the differences came from the reinforcing details. Each specimen was made up of two precast beam units and two end columns stubs, and the precast components were assembled in the joint region through cast-in-situ concrete. The span for the beams was 2750 mm, while the cross-section dimensions were 300 × 150 mm for beams, 250 × 250 mm for middle columns and 400 × 450 mm for end column stubs. Two kinds of reinforcing details were used in the connection region, namely, hooked (90° bent) and lap-spliced, as shown in Fig. 5. Apart from the reinforcing details, the main investigating parameter was the reinforcing ratio, which is listed in Table 2.

The material properties of the specimens, including concrete and reinforcement, are given in Table 3, where bar H13 and H16 marked with * were used for specimen MJ-B-1.19/0.59R only. The two end column stubs were restrained each by two load cells in in the horizontal direction, and one pin support in the vertical direction. In addition, two sets of steel columns were arranged on each side of the middle span of the beams to prevent out-of-plane failure of the specimens. Column removal was simulated through gradually increasing the vertical displacement at the top of the middle column stub. More details about the experiments can be found in (Kang and Tan 2015a; Kang et al. 2015).

Analysis results

The established numerical model is demonstrated in Fig. 6. The beams and columns are modeled with fiber elements, and the joints are represented with the Joint2D model discussed above. The finite element mesh size is defined as the section height to avoid softening localization issue (Feng et al. 2015), and two integration points are used for each element. The sections are divided into two parts, i.e., the precast part and the cast-in-situ part, and each part is discretized into 20 concrete fibers, and the number and locations of the steel fibers are assigned according to the reinforcement detail of each beam and column. Material model parameters are determined according to Table 2, and the concrete tensile strength is given by $0.25\sqrt{f_c}$, where f_c is the compressive strength. The confinement effect is considered through Mander model (Mander et al. 1988). The embedded length for the continuous reinforcement bars is set as half of the column width, i.e., 125 mm, and for the bent bar it is $190+5d_b$ mm and for the lap-spliced bar it is 470 mm. The boundary conditions of the end column stubs are simulated with lateral elastic springs, and the stiffness is assumed to be the level of 10^5 kN/m, which is consistent with the recommendation in (Yu and Tan 2013) based on the measurement of the reaction forces and the displacements. Vertical load is applied at the top of the middle column stub through displacement control, and for a quasi static analysis the time step is set as 1 mm/s.

The simulated vertical displacement of the middle column versus the vertical applied load on the column top, as well as the horizonal reaction forces of the beams (or the beam axial forces) of all the six specimens are plotted against the experimental results in Fig. 7. Good agreements are achieved between the numerical and experimental results for nearly all the specimens. It can be found from the applied load-vertical displacement curves that the initial stiffness, flexural beam action, and the effects of compressive arch action (CAA) and catenary action all can be well reflected by the numerical model. Furthermore, the bar fracture failure at the middle column joint and end column stubs can also be reproduced.

More specifically, the CAA capacities predicted by the numerical model for specimens MJ-B-0.52/0.35S, MJ-B-0.88/0.59R, MJ-B-1.19/0.59R and MJ-L-0.52/0.35S are nearly the same as the experimental results, while they are 6 kN and 8.3 kN larger than the experimental values for specimens MJ-L-0.88/0.59R and MJ-L-1.19/0.59R, respectively, which corresponds to the relative differences of 11% and 14% between the numerical and experimental results. The numerical models also predict quite well the bar fracture at the middle and end column joints for specimens MJ-B-0.52/0.35S, MJ-B-1.19/0.59R and MJ-L-0.52/0.35S and MJ-L-1.19/0.59R, while the results for specimens MJ-B-0.88/0.59R and MJ-L-0.88/0.59R are less comparable with the experimental ones. This may be caused by the uncertainty in material properties, especially the fracture strain of the reinforcement bars.

For the horizonal reaction force curves, the numerical results also exhibit good agreement with the experimental results. Take the specimen MJ-B-0.88/0.59R as an example, the beam axial force is first under compression and then transits to tension due to catenary action from a displacement around 350 mm. The calculated maximum compression force is 282.7 kN which matches almost exactly the measured value of 282.5 kN. Fig. 8 also gives the comparison of the deformed profile of specimen MJ-B-0.88/0.59R under different vertical displacements obtained from the numerical model and the experiment. As can be seen in the figure, the two sets of results match well with each other. In general, the numerical results indicate that the developed finite element model can predict realistically the responses of precast RC frame sub-assemblages, and therefore can be used as an effective tool in a progressive collapse analysis.

PARAMETRIC STUDIES ON PROGRESSIVE COLLAPSE BEHAVIOR OF PRECAST RC SUB-ASSEMBLAGES

With the validated numerical model, parametric studies can be performed to investigate the influences of a variety of factors on the progressive collapse behavior of the precast RC sub-assemblages. It is worth noting at this juncture that many basic design parameters, including reinforcement ratio, beam depth, concrete strength, slab effect, boundary condition, etc., have been widely studied before (Yu and Tan 2013; Yu and Tan 2014; Pham et al. 2016). The present study therefore mainly focuses on a few factors that are particularly important for the analysis of precast RC structures, namely, the modeling strategies, the strength of the cast-in-situ concrete, and the anchorage length of the reinforcement bars at the joint region. To concentrate the observation to these factors, the specimen MJ-L-0.88/0.59R is selected as a reference case to conduct the parametric studies as described in the following subsections.

Effect of modeling strategies

First the effect of modeling strategies is discussed. The modeling strategy with elastic shear spring as used in the above validation analysis is denoted as Model 1. To study the influence of shear deformation at the joint region, Model 2 adopts a nonlinear shear spring property, which can be obtained from MCFT. Model 3 employs a rigid joint model to investigate the influence of the bond-slip effect, which means beam interface springs in the Joint2D model are set as rigid and the bond-slip effect is neglected. Model 4 removes the Joint2D element and uses fiber element only to simulate the sub-assemblages to improve the computational efficiency. However, to consider the bond-slip effect, the stress-strain relationship of reinforcement in the critical nonlinear region is modified by assuming that the equivalent strain is the sum of the slip and the bar deformation (Bao et al. 2012), i.e., $\epsilon' = \epsilon + s/L_p$, where s is the bar slip derived above and L_p is the critical nonlinear region length, usually equals beam height.

The results for the four models are demonstrated in Fig. 9. As can be seen in the figure, the results by Model 1 and Model 2 are nearly the same, which indicates that considering the shear deformation actually has little influence on the analysis of progressive collapse behavior of precast concrete structures. This conclusion echoes closely observations made in previous researches by (Bao et al. 2008; Yu and Tan 2013; Yu and Tan 2014; Rashidian et al. 2016). Model 3 appears to overestimate the CAA capacity of the specimen, and the bar fracture occurs earlier than the other two models since the fixed-end rotation caused by bar slip at the beam interface is not accounted for in Model 3. On the other hand, Model 1 and Model 4 predict almost the same results, which means developing an equivalent reinforcement model including bond-slip is an alternative way for modeling precast frame sub-assemblage under progressive collapse, and the computational efficiency can be also improved.

Effect of concrete strength in cast-in-situ region

Precast concrete structures enables us using concrete of different grades as the cast-in-situ part to improve the integrity of the structure. Therefore, the influence of concrete strength on the progressive collapse resistance is studied. The original concrete strength for the cast-in-situ part in specimen MJ-L-0.88/0.59R is 20.3 MPa, and now cast-in-situ part of 30 MPa and 40 MPa is also simulated. The numerical results are demonstrated in Fig. 10. With the increase of the concrete strength, the CAA capacity will increases; however, the degree of the increase appears to be very limited. Meanwhile, increasing the concrete strength makes little difference to the catenary action, and this is expected since catenary action is mainly controlled by the reinforcement properties. It should be noted that the onset of the bar fracture at the middle column interface becomes earlier with the increase of the concrete strength. This is because the bond strength will rise as the concrete strength increases, resulting in the fracture of bar at a smaller rotation of the beams.

Effect of beam bar properties

The bottom bar directly affect the progressive collapse behavior of the precast assemblages, and it is also closely related to the bond strength in the joint region. Hence the bar diameter and bar strength are studied. The specimen MJ-L-0.88/0.59R is still set as the reference model, in which the bar diameter and yielding strength are 13 mm and 470 MPa, respectively. Then the model is first varied into two new models using different bar diameters, namely 10 mm and 16 mm, respectively, while the bar yield strength remains at 470 MPa. Subsequently, the reference model is varied into another two models using two yielding strengths of 520 MPa and 570 MPa, respectively, while other properties remain unchanged.

The numerical results are shown in Fig. 11 and 12. As can generally be expected, the bar diameter, which in the case herein also represents the amount of reinforcement, has a direct influence on the progressive collapse behavior of the sub-assemblage. The CAA capacity and catenary action capacity both increase with the increase of the bar diameter (and hence amount of reinforcement herein), since the total axial strengths of the beams are controlled by the reinforcing bars. Compared with the reference model, the CAA capacity of the model with a smaller 10-mm bar decreases by 32.1%, while that with a larger 16-mm bar increases by 33.8%. The respective catenary action decreased by 46.8% and increased by 53.4%. Meanwhile, the onset of the transition of the horizonal beam force from compression to tension becomes earlier for model with increased reinforcement, as shown in Fig. 12(b). The concrete will crush earlier for model with larger amount of reinforcement, correspondingly the horizontal force will change to tension earlier.

In a similar trend, with the increase of the bar yielding strength, the CAA capacity and catenary action capacity also exhibit a significant increase, as shown in Fig. 12. With the yield strength increasing from 470 MPa to 520 MPa and 570 MPa, the CAA capacities increase by 8.5% and 16.9%, respectively.

The above results indicates that both the CAA and the catenary capacities tend to increase consistently with the increase of the total strength of the steel reinforcement. Since the total reinforcement strength is closely correlated to the flexural strength of the section, in general design procedure for a precast structure, a certain required degree of progressive collapse resistance may be achieved through controlling the flexure strength of the section, within a reasonable reinforcement ratio range.

Effect of anchorage length at the joint

The anchorage length in the joint region is a crucial point for the precast RC sub-assemblage under progressive collapse since it is directly related with the integrity of the joint. Sufficient anchorage length of the bar at the joint will avoid pull-out failure. The original anchorage length for specimen MJ-L-0.88/0.59R is 470 mm. Here variations to 370 mm, 270 mm and 170 mm, respectively, are also simulated. Fig. 13 presents the numerical results for the models with different anchorage lengths. With shorter anchorage length (170 mm and 270 mm), the failure mode of the bar at the middle beam-to-column joint is bar pull-out, while it changes to bar fracture for the cases of anchorage length 370 mm and above. The results for anchorage length 370 mm and 470 mm are basically the same since the anchorage length is sufficient to develop the bond behavior, and thus the generated bond-slip spring property in the Joint2D element are the same. However, for anchorage length 170 mm and 270 mm, pull-out failure will occur prior to fracture according to the derived stress-slip behavior of reinforcement in this paper. Therefore, the failure of the beam interface spring in Joint2D element of this case corresponds to the pull-out failure of the reinforcement bars. However, for all the cases, the ultimate catenary capacities are very close since at this stage the bottom bars all failed (either due to pull-out or due to fracture) and the final catenary capacity is actually determined by the tensile force of the top bars, which is continuous in the models. In general, insufficient anchorage length for the bottom bars will cause pull-out failure at the middle joint, and the beam end flexural capacity will also be reduced due to the failure of the bottom bars.

CONCLUSIONS

In this paper, an efficient numerical model is developed for the progressive collapse analysis of precast RC sub-assemblages. The model is based on the fiber element and Joint2D element in OpenSEES. In particular, to account for the significant bond-slip effect in precast RC structures, the reinforcement stress-slip relationship is analytically derived, and different anchorage types and lengths are considered. To validate the numerical model, a set of recently reported experiments of six precast RC sub-assemblages under a middle column removal scenario are simulated. The results indicate that the proposed model can well capture the typical progressive collapse behaviors of the precast RC structures, including behaviors in the flexural, CAA, and catenary stages.

With the validated numerical model, several important factors influencing the analysis of precast structures are investigated, these include the modeling strategy, the post-cast concrete strength, the bar diameter and yielding strength (or total reinforcement contributions), and the bottom bar anchorage length. The results indicate that the bond-slip effect has a sensible influence and therefore should be considered in the numerical model; otherwise the CAA capacity will be overestimated and the beam end rotation capacity will be underestimated. Improving the concrete strength of cast-in-situ part will increase the CAA capacity, but the extent appears to be limited. The reinforcement altogether, through bar diameter and yielding strength, will have a great influence on the CAA capacity as well as the catenary capacity. These two capacities will increase consistently with increasing the bar diameter and yielding strength; but the onset of beam horizontal force transition from compression to tension will also become earlier. The failure mode of the bar at the middle column joint depends on the anchorage length. Pull-out failure will happen for insufficient anchorage length and fracture failure will happen for sufficient anchorage length. However, in both cases the final catenary action capacity is nearly the same in principle since it is dominated by the tensile force of the top bars.

In general, the numerical model developed in this paper represents a balanced consideration between the analysis accuracy and computational efficiency. The proposed model approach can be used as an effective tool for progressive collapse analysis of precast structures. It should be noted that some other detailed aspects relating to precast RC structures, like the interface between precast and cast-in-situ concrete surfaces and the bond deterioration, still requires further study in order to be considered in the numerical model.

ACKNOWLEDGEMENTS

The authors would like to acknowledge financial supports from the National Key Research and

Development Program of China (No. 2016YFC0701400), the National Natural Science Foundation of China (Grant No. 51708106), the Natural Science Foundation of Jiangsu Province (Grant No. BK20170680), and the Fundamental Research Funds for the Central Universities (Nos. 2242017k30002, 2242017k40212).

APPENDIX I. CONCRETE DAMAGE-PLASTICITY MODEL

The uniaxial concrete model used in this paper is based on damage mechanics, and the general form of the constitutive relation can be written as

$$\sigma^{\pm} = \left(1 - d^{\pm}\right) E_c \left(\epsilon^{\pm} - \epsilon^{p\pm}\right) = \left(1 - d^{\pm}\right) E_c \epsilon^{e\pm} \tag{16}$$

where $\sigma^{\pm}$ is the stress; $\epsilon^{\pm}$ is the total strain; $\epsilon^{p\pm}$ is the plastic strain; $d^{\pm}$ is the damage variable; E_c is the elastic modulus; the superscript $\pm$ indicate tension and compression, respectively.

The damage evolution can be determined by either micro-mechanics (Feng et al. 2016b) or experimental data (Feng et al. 2017), here the latter one is adopted

$$d^{\pm} = \begin{cases} 1 - \frac{\rho^{\pm} n^{\pm}}{n^{\pm} - 1 + (x^{\pm})^{n^{\pm}}} & x^{\pm} \leq 1 \\ 1 - \frac{\rho^{\pm}}{\alpha^{\pm}(x^{\pm} - 1)^2 + x^{\pm}} & x^{\pm} > 1 \end{cases} \tag{17}$$

and the symbols are defined as

$$x^{\pm} = \frac{\epsilon^{e\pm}}{\epsilon_c^{\pm}}, \quad \rho^{\pm} = \frac{f_c^{\pm}}{E_c \epsilon_c^{\pm}}, \quad n^{\pm} = \frac{E_c \epsilon_c^{\pm}}{E_c \epsilon_c^{\pm} - f_c^{\pm}} \tag{18}$$

where $f_c^{\pm}$ and $\epsilon_c^{\pm}$ are the stress and strain corresponding to the peak strength in tension and compression; E_c is the elastic modulus.

The plastic strains are also given by an empirical model, i.e.,

$$\begin{cases} \epsilon^{p+} = 0 \\ \epsilon^{p-} = \xi_p \left(d^{-}\right)^{\eta_p} \end{cases} \tag{19}$$

where ξ_p and η_p are the plastic parameters that controls the plastic evolution, and the recommended values are 0.6 and 0.1, respectively. Note that the tensile plastic strain is neglected since it is relatively small and has little influence on the overall behavior of concrete.

APPENDIX II. BILINEAR REINFORCEMENT MODEL

The bilinear model is used for reinforcement bars. The stress-strain relation under tension and compression is assumed to be the same, and is given by

$$\sigma_s = \begin{cases} E_s \epsilon_s & \epsilon_s \leq \epsilon_y \\ f_y + E_h \left(\epsilon_s - \epsilon_y\right) & \epsilon_s > \epsilon_y \end{cases} \tag{20}$$

where E_s is the elastic modulus; f_y and ϵ_y are the yielding strength and strain, respectively; $E_h = bE_s$ is the hardening modulus; b is the hardening ratio.

REFERENCES

Altoontash, A. (2004). "Simulation and damage models for performance assessment of reinforced concrete beam-column joints." Ph.D. thesis, Stanford University, Stanford University.

Bao, Y., Kunnath, S. K., El-Tawil, S., and Lew, H. S. (2008). "Macromodel-based simulation of progressive collapse: Rc frame structures." *Journal of Structural Engineering*, 134(7), 1079–1091.

Bao, Y., Lew, H., and Kunnath, S. K. (2012). "Modeling of reinforced concrete assemblies under column-removal scenario." *Journal of Structural Engineering*, 140(1), 04013026.

Brunesi, E. and Nascimbene, R. (2014). "Extreme response of reinforced concrete buildings through fiber force-based finite element analysis." *Engineering Structures*, 69, 206–215.

Brunesi, E., Nascimbene, R., Parisi, F., and Augenti, N. (2015). "Progressive collapse fragility of reinforced concrete framed structures through incremental dynamic analysis." *Engineering Structures*, 104, 65–79.

Brunesi, E. and Parisi, F. (2017). "Progressive collapse fragility models of european reinforced concrete framed buildings based on pushdown analysis." *Engineering Structures*, 152, 579–596.

DoD (2013). "Unified facilities criteria: design of buildings to resist progressive collapse." *Report No. UFC 4-023-03*, Department of Defense, Washington DC, United States.

Ellingwood, B. R. (2006). "Mitigating risk from abnormal loads and progressive collapse." *Journal of Performance of Constructed Facilities*, 20(4), 315–323.

Feng, D.-C., Kolay, C., Ricles, J. M., and Li, J. (2016a). "Collapse simulation of reinforced concrete frame structures." *The Structural Design of Tall and Special Buildings*, 12(25), 578–601.

Feng, D.-C., Ren, X., and Li, J. (2015). "Implicit gradient delocalization method for force-based frame element." *Journal of Structural Engineering*, 142(2), 04015122.

Feng, D.-C., Ren, X., and Li, J. (2016b). "Stochastic damage hysteretic model for concrete based on micromechanical approach." *International Journal of Non-Linear Mechanics*, 83, 15–25.

Feng, D.-C., Wu, G., Sun, Z.-Y., and Xu, J.-G. (2017). "A flexure-shear timoshenko fiber beam element based on softened damage-plasticity model." *Engineering Structures*, 140, 483–497.

GSA (2013). "Alternate path analysis & design guidelines for progressive collapse resistance." *Report no.*, General Service Administration, Washington DC, United States.

Hsu, T. T. (1988). "Softened truss model theory for shear and torsion." *ACI Structural Journal*, 85(6).

Kang, S.-B. and Tan, K.-H. (2015a). "Behaviour of precast concrete beam–column sub-assemblages subject to column removal." *Engineering Structures*, 93, 85–96.

Kang, S.-B. and Tan, K.-H. (2015b). "Bond–slip behaviour of deformed reinforcing bars embedded in well-confined concrete." *Magazine of Concrete Research*, 68(10), 515–529.

Kang, S.-B. and Tan, K.-H. (2017). "Progressive collapse resistance of precast concrete frames with discontinuous reinforcement in the joint." *Journal of Structural Engineering*, 143(9), 04017090.

Kang, S.-B., Tan, K.-H., and Yang, E.-H. (2015). "Progressive collapse resistance of precast beam–column sub-assemblages with engineered cementitious composites." *Engineering Structures*, 98, 186–200.

Li, Y., Lu, X., Guan, H., and Ren, P. (2016a). "Numerical investigation of progressive collapse resistance of reinforced concrete frames subject to column removals from different stories."

Advances in Structural Engineering, 19(2), 314–326.

Li, Y., Lu, X., Guan, H., Ren, P., and Qian, L. (2016b). “Probability-based progressive collapse-resistant assessment for reinforced concrete frame structures.” *Advances in Structural Engineering*, 19(11), 1723–1735.

Li, Y., Lu, X., Guan, H., and Ye, L. (2011). “An improved tie force method for progressive collapse resistance design of reinforced concrete frame structures.” *Engineering Structures*, 33(10), 2931–2942.

Lowes, L. N. and Altoontash, A. (2003). “Modeling reinforced-concrete beam-column joints subjected to cyclic loading.” *Journal of Structural Engineering*, 129(12), 1686–1697.

Lu, X., Lin, K., Li, Y., Guan, H., Ren, P., and Zhou, Y. (2016). “Experimental investigation of rc beam-slab substructures against progressive collapse subject to an edge-column-removal scenario.” *Engineering Structures*.

Mander, J. B., Priestley, M. J., and Park, R. (1988). “Theoretical stress-strain model for confined concrete.” *Journal of Structural Engineering*, 114(8), 1804–1826.

Ministry of Construction of the People’s Republic of China, B. (2010). “Code for design of concrete structures.” *Gb50010-2010*, Beijing, China.

Pham, A.-T., Tan, K.-H., and Yu, J. (2016). “Numerical investigations on static and dynamic responses of reinforced concrete sub-assemblages under progressive collapse.” *Engineering Structures*.

Qian, K. and Li, B. (2011). “Experimental and analytical assessment on rc interior beam-column subassemblages for progressive collapse.” *Journal of Performance of Constructed Facilities*, 26(5), 576–589.

Qian, K. and Li, B. (2012). “Performance of three-dimensional reinforced concrete beam-column substructures under loss of a corner column scenario.” *Journal of Structural Engineering*, 139(4), 584–594.

Qian, K., Li, B., and Zhang, Z. (2016). “Influence of multicolumn removal on the behavior of rc floors.” *Journal of Structural Engineering*, 142(5), 04016006.

Rashidian, O., Abbasnia, R., Ahmadi, R., and Nav, F. M. (2016). "Progressive collapse of exterior reinforced concrete beam–column sub-assemblages: Considering the effects of a transverse frame." *International Journal of Concrete Structures and Materials*, 10(4), 479–497.

Ren, P., Li, Y., Lu, X., Guan, H., and Zhou, Y. (2016). "Experimental investigation of progressive collapse resistance of one-way reinforced concrete beam–slab substructures under a middle-column-removal scenario." *Engineering Structures*, 118, 28–40.

Sasani, M. and Kropelnicki, J. (2008). "Progressive collapse analysis of an rc structure." *The Structural Design of Tall and Special Buildings*, 17(4), 757–771.

Sasani, M., Werner, A., and Kazemi, A. (2011). "Bar fracture modeling in progressive collapse analysis of reinforced concrete structures." *Engineering Structures*, 33(2), 401–409.

Sezen, H. and Setzler, E. J. (2008). "Reinforcement slip in reinforced concrete columns." *ACI Structural Journal*, 105(3), 280.

Su, Y., Tian, Y., and Song, X. (2009). "Progressive collapse resistance of axially-restrained frame beams." *ACI Structural Journal*, 106(5), 600.

Valipour, H. R. and Foster, S. J. (2010). "Finite element modelling of reinforced concrete framed structures including catenary action." *Computers & structures*, 88(9), 529–538.

Vecchio, F. J. and Collins, M. P. (1986). "The modified compression-field theory for reinforced concrete elements subjected to shear." *ACI Structural Journal*, ACI, 83(2), 219–231.

Yap, S. L. and Li, B. (2011). "Experimental investigation of reinforced concrete exterior beam-column subassemblages for progressive collapse." *ACI Structural Journal*, 108(5), 542.

Yi, W.-J., He, Q.-F., Xiao, Y., and Kunnath, S. K. (2008). "Experimental study on progressive collapse-resistant behavior of reinforced concrete frame structures." *ACI Structural Journal*, 105(4), 433.

Yu, J. and Tan, K.-H. (2013). "Experimental and numerical investigation on progressive collapse resistance of reinforced concrete beam column sub-assemblages." *Engineering Structures*, 55, 90–106.

Yu, J. and Tan, K.-H. (2014). "Numerical analysis with joint model on rc assemblages subjected to progressive collapse." *Magazine of Concrete Research*, 66(23), 1201–1218.

Yu, X. H., Lu, D. G., Qian, K., and Li, B. (2016). "Uncertainty and sensitivity analysis of reinforced concrete frame structures subjected to column loss." *Journal of Performance of Constructed Facilities*, 04016069.

List of Tables

TABLE 1. Summary of the proposed modeling approach

Member	Element	Material	
Beams/columns	DB fiber element	Concrete fibers	ConcreteD
		Steel fibers	Steel01
Beam-to-column connection	Joint2D element	Shear panel	Elastic
		Column interface	Rigid
		Beam interface	Hysteretic

TABLE 2. Reinforcing details of the tested specimens

Specimen	Curtailed bar length (mm)	A-A section		B-B section	
		Top	Bottom	Top	Bottom
MJ-B-0.52/0.35S	900	3H10	2H10	2H10	2H10
MJ-B-0.88/0.59R	1000	3H13	2H13	2H13	2H13
MJ-B-1.19/0.59R	1000	2H16+H13	2H13	2H16+H13	2H13
MJ-L-0.52/0.35S	900	3H10	2H10	2H10	2H10
MJ-L-0.88/0.59R	1000	3H13	2H13	2H13	2H13
MJ-L-1.19/0.59R	1000	2H16+H13	2H13	2H16+H13	2H13

TABLE 3. Material properties of the tested specimens

Bar type	Reinforcement				
	d_b (mm)	f_y (MPa)	f_u (MPa)	E_s (MPa)	ϵ_u (%)
H10	10	462	553	187302	11.9
H13	13	471	568	186526	12.2
H16	16	527	618	196341	11.9
H13*	13	549	698	206600	16.3
H16*	16	573	674	211300	12.9

Specimen	Concrete strength (MPa)	
	Precast units	Cast-in-situ
MJ-B-0.52/0.35S	27.9	35.8
MJ-B-0.88/0.59R	27.9	20.3
MJ-B-1.19/0.59R	40.5	36.1
MJ-L-0.52/0.35S	27.9	35.8
MJ-L-0.88/0.59R	27.9	20.3
MJ-L-1.19/0.59R	27.9	20.3

List of Figures

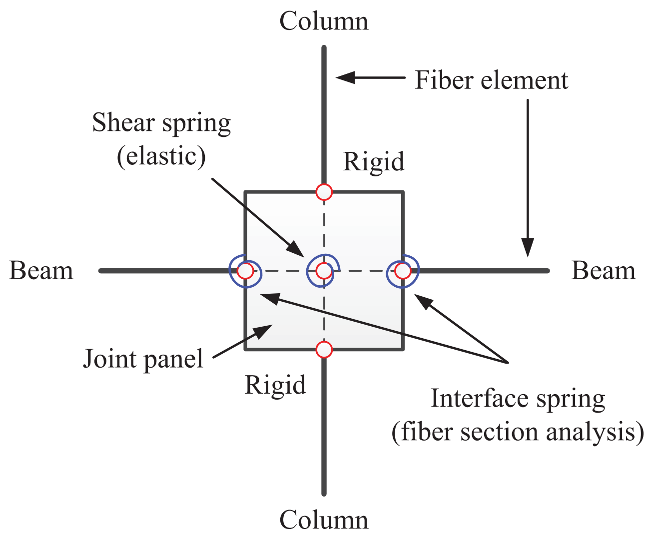

Fig. 1. Joint2D element for precast sub-assemblage under progressive collapse

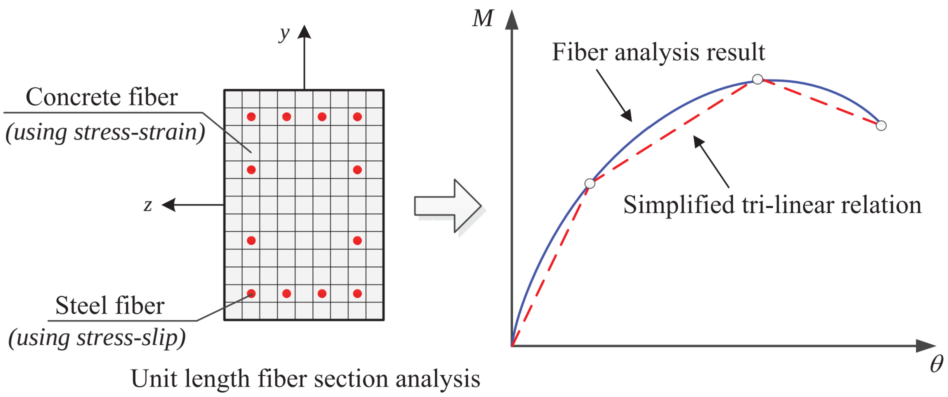

Fig. 2. Determination of the beam end spring property through fiber section analysis

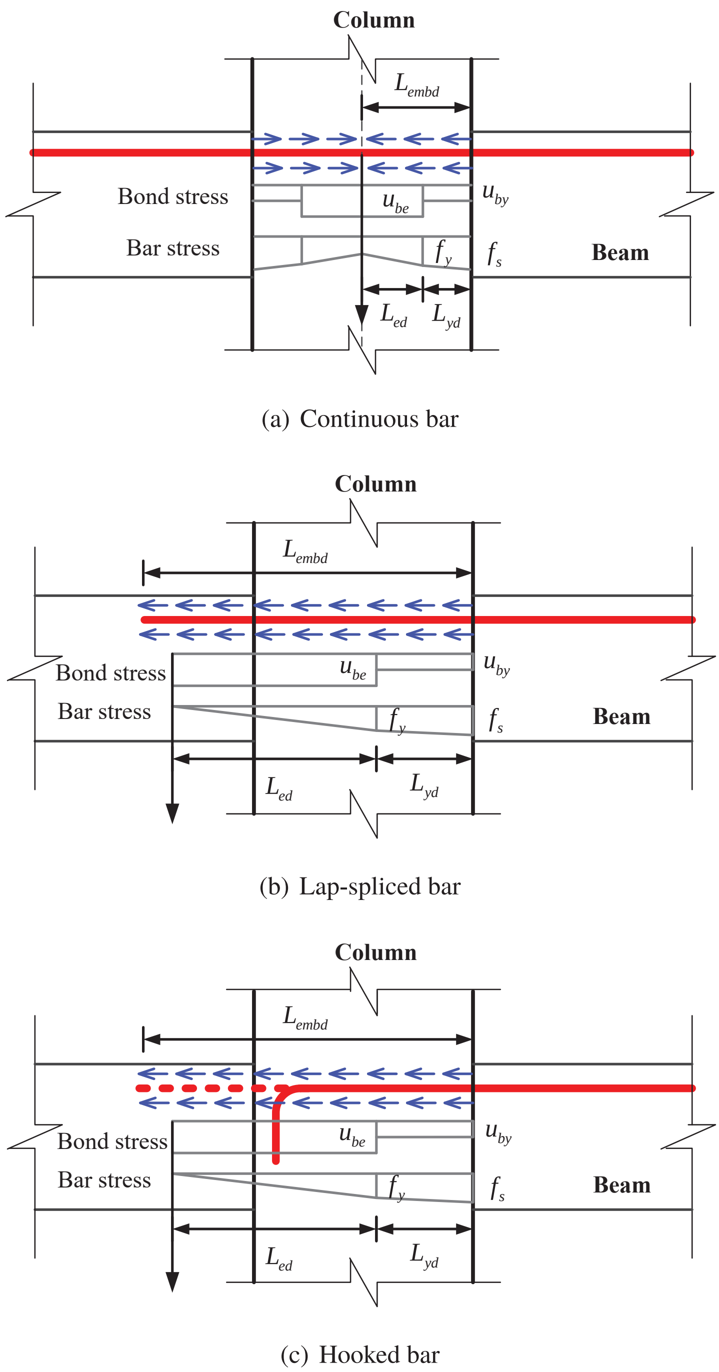

Fig. 3. Bond and stress profile of different anchorage types for the precast sub-assemblage

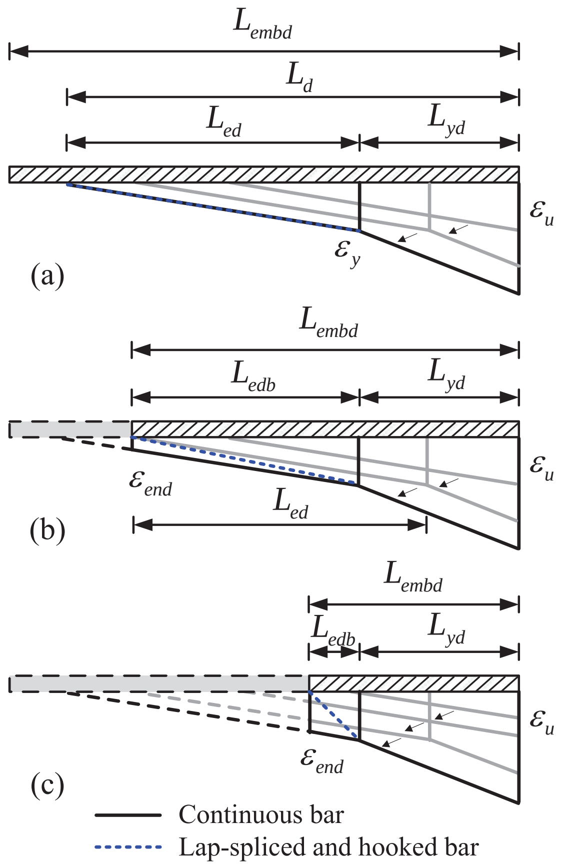

Fig. 4. Strain profiles of different bar embedded length

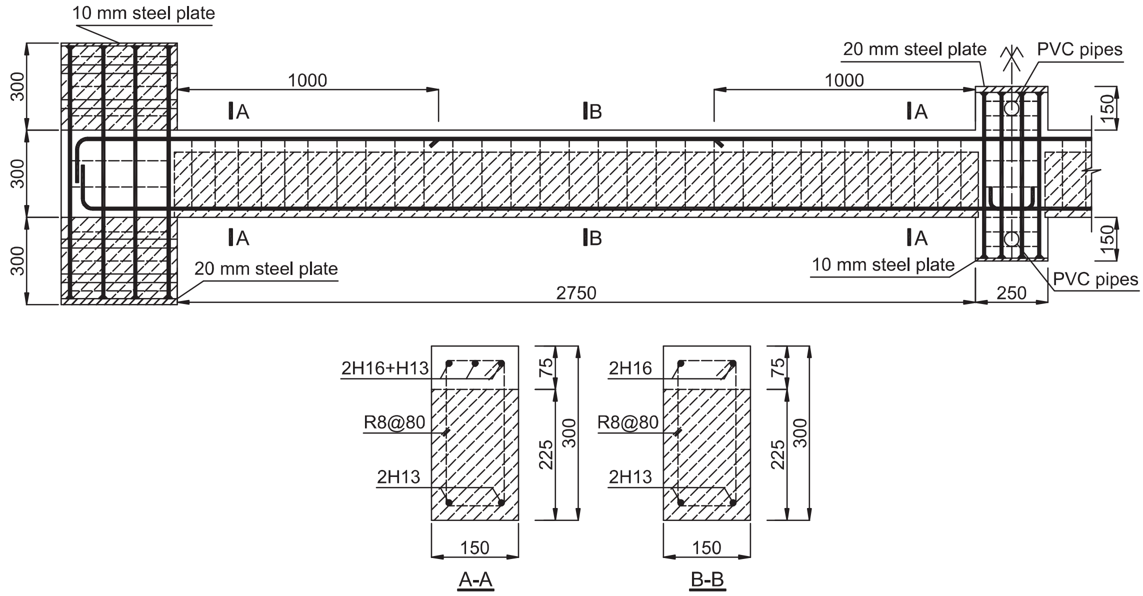

(a) Hooked bottom reinforcement

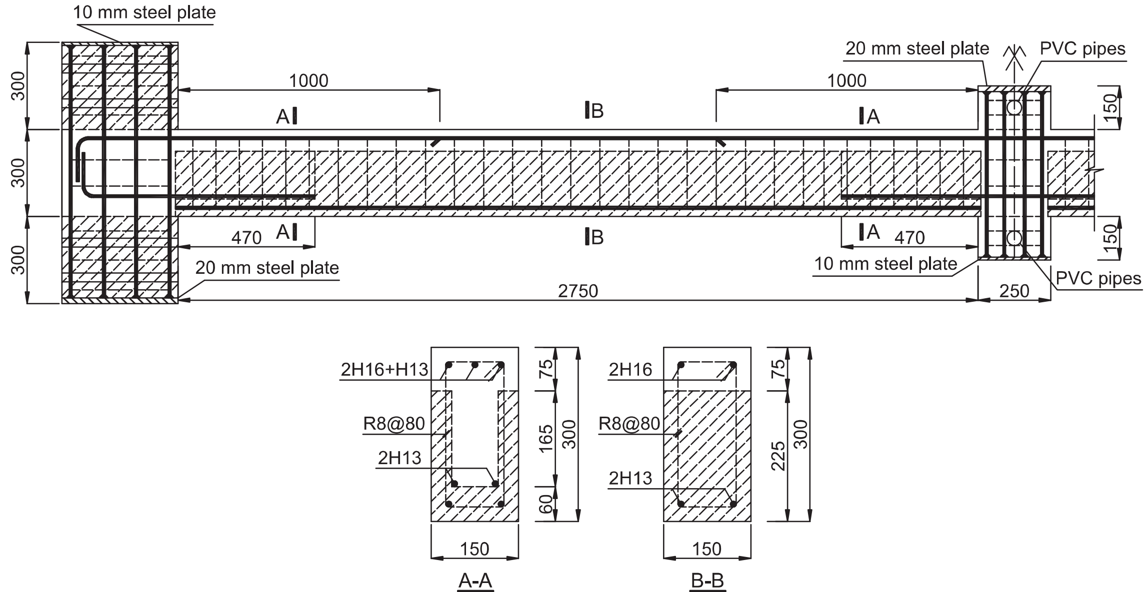

(b) Lap-spliced bottom reinforcement

Fig. 5. Experiments of precast sub-assemblages subjected to progressive collapse by Kang and Tan

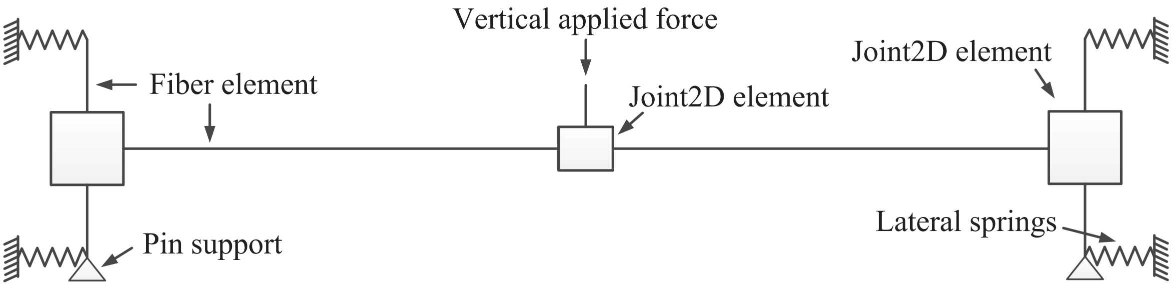

Fig. 6. Established finite element model

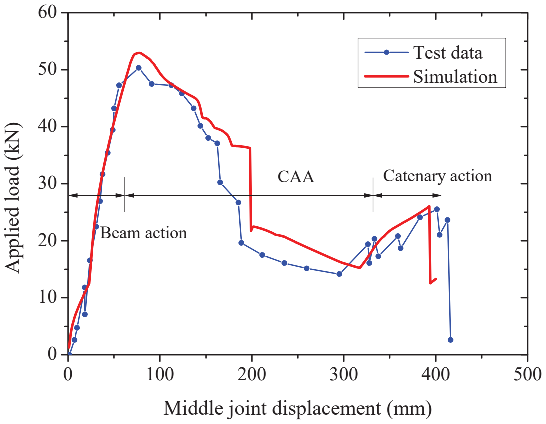

(a) MJ-B-0.52/0.35S-vertical

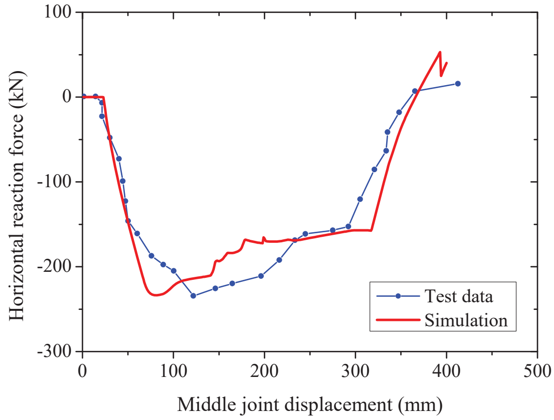

(b) MJ-B-0.52/0.35S-horizonal

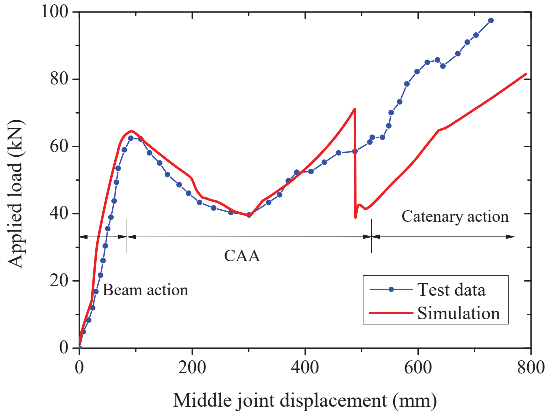

(c) MJ-B-0.88/0.59R-vertical

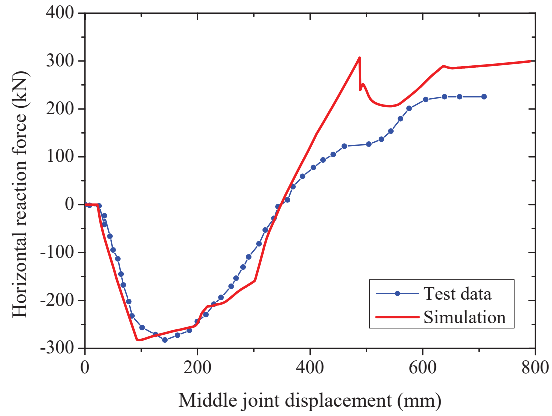

(d) MJ-B-0.88/0.59R-horizonal

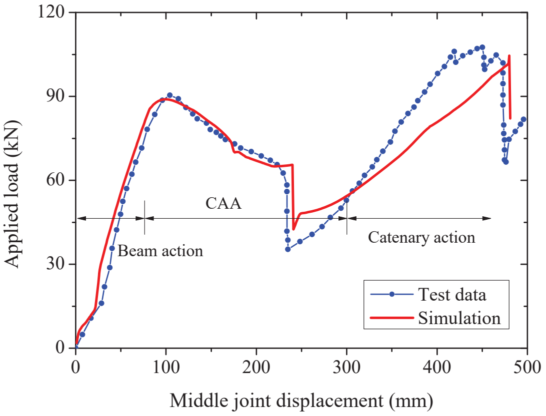

(e) MJ-B-1.19/0.59R-vertical

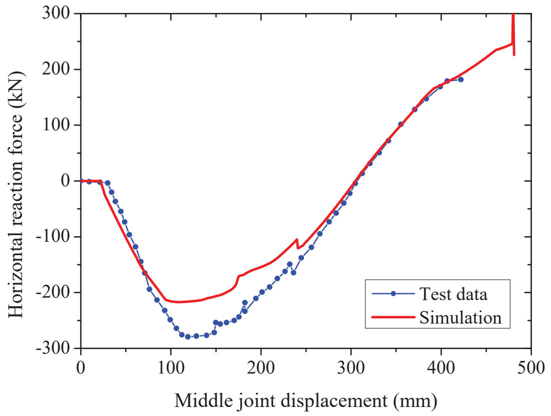

(f) MJ-B-1.19/0.59R-horizonal

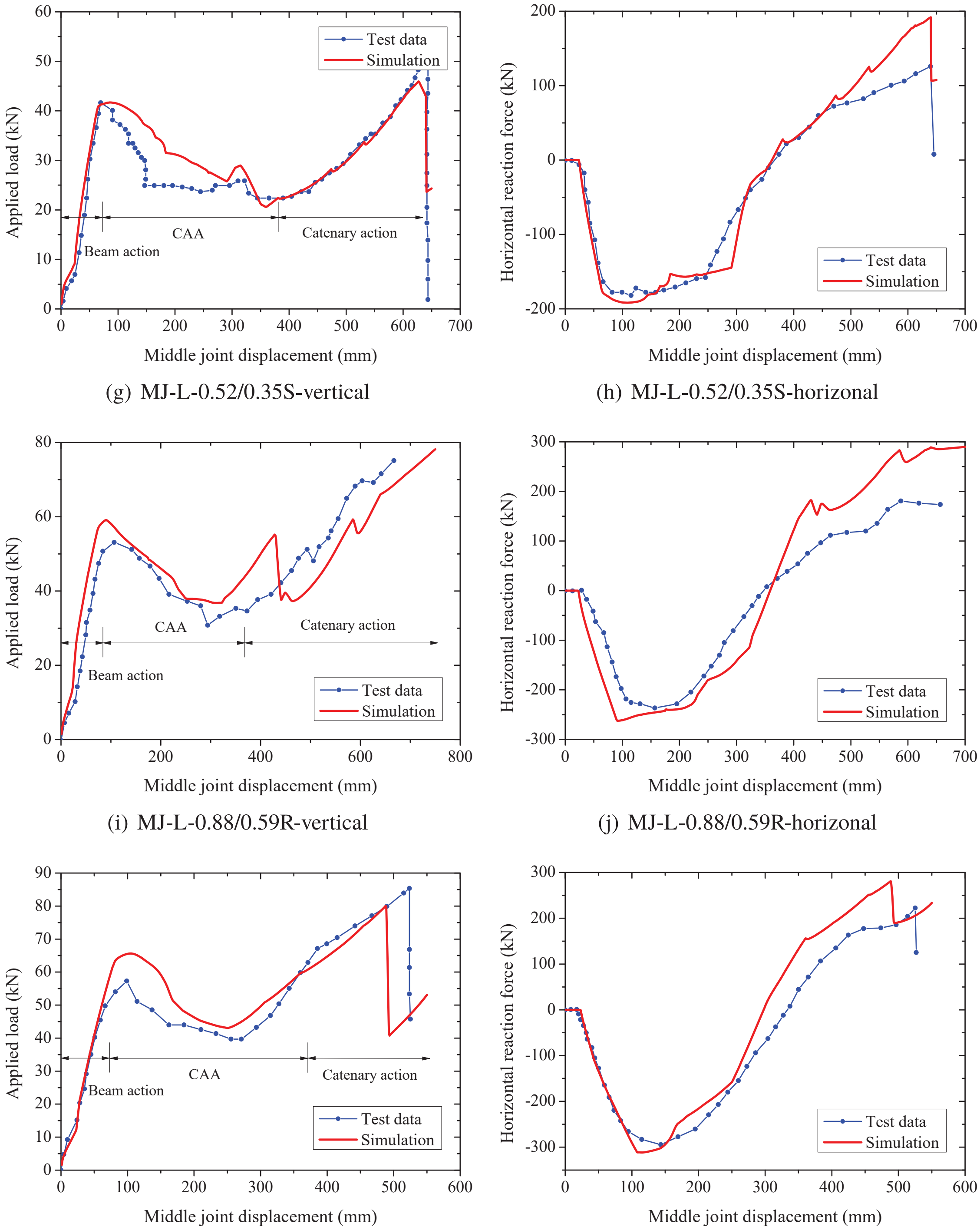

(g) MJ-L-0.52/0.35S-vertical (h) MJ-L-0.52/0.35S-horizonal

(i) MJ-L-0.88/0.59R-vertical (j) MJ-L-0.88/0.59R-horizonal

(k) MJ-L-1.19/0.59R-vertical (l) MJ-L-1.19/0.59R-horizonal

Fig. 7. Comparison of numerical and experimental results

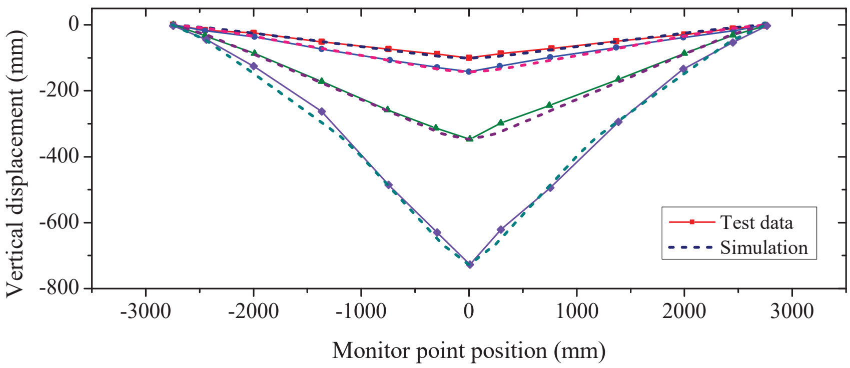

Fig. 8. Deformed profile for specimen MJ-B-0.88/0.59R

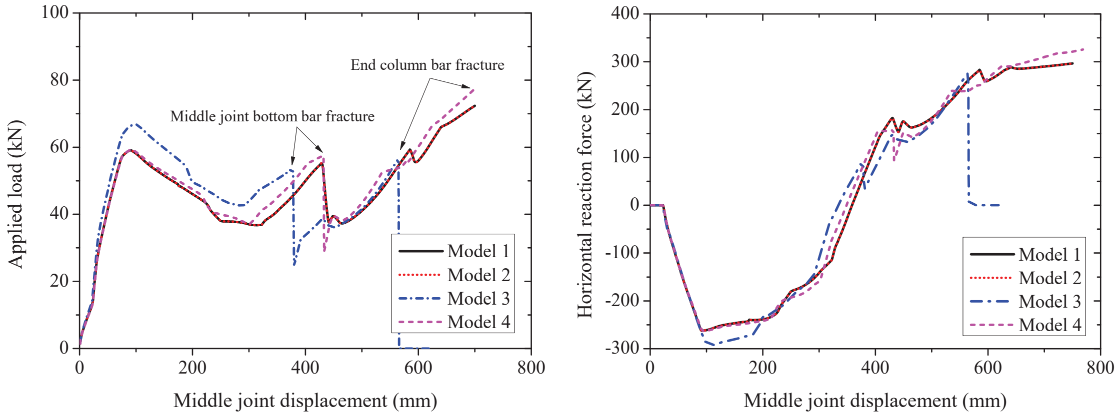

(a) Applied load-vertical displacement (b) Horizonal force-vertical displacement

Fig. 9. Numerical results for different modeling strategies

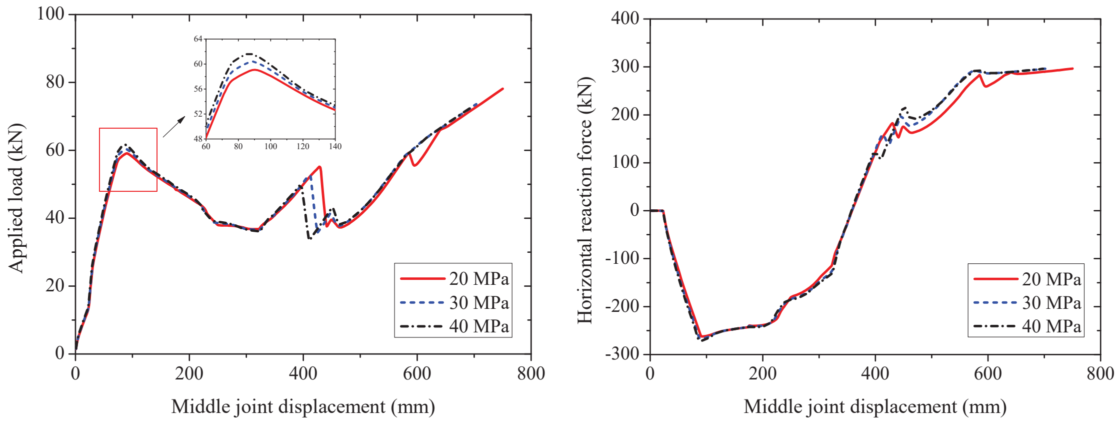

(a) Applied load-vertical displacement

(b) Horizonal force-vertical displacement

Fig. 10. Numerical results for cast-in-situ concrete with different strengths

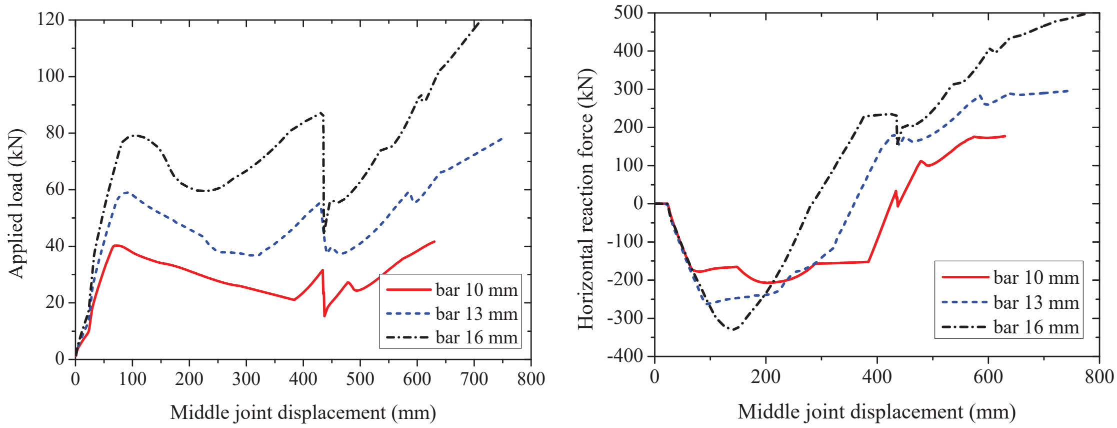

(a) Applied load-vertical displacement

(b) Horizonal force-vertical displacement

Fig. 11. Numerical results for different bar diameters

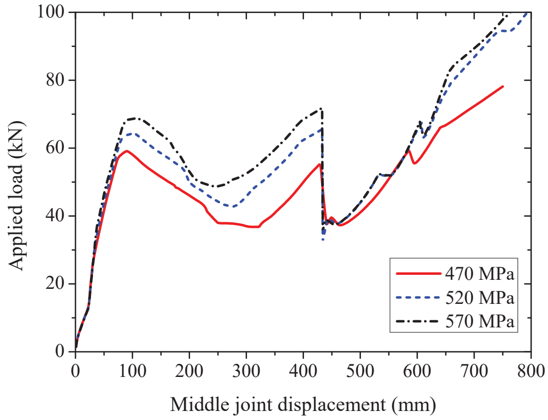

(a) Applied load-vertical displacement

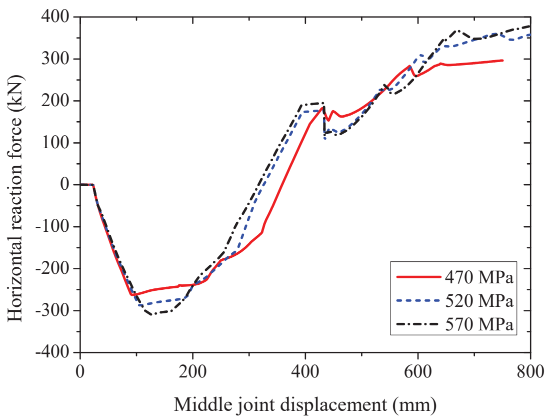

(b) Horizonal force-vertical displacement

Fig. 12. Numerical results for different bar yielding strengths

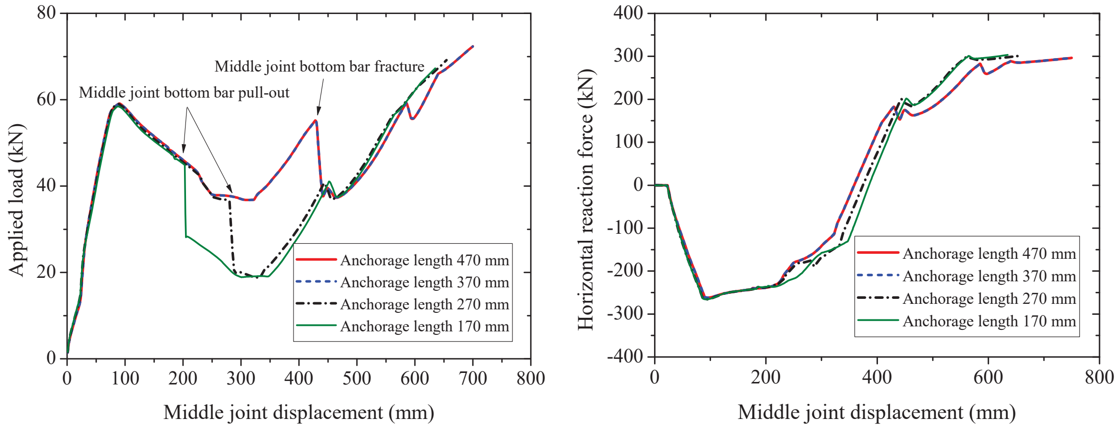

(a) Applied load-vertical displacement (b) Horizonal force-vertical displacement

Fig. 13. Numerical results for different anchorage length